

CFD INVESTIGATION ON THE AERODYNAMIC CHARACTERISTICS ANALYSIS OF A NANO -SIZED WINDTURBINE APPLIED COMSOL

C.THIRUVASAGAM¹, S.SARAVANAN², VAIRAVEL .M³, SACHIN S RAJ⁴

¹Assistant Professor , Department of Mechanical Engineering , Gnanamani College of Technology ,Namakkal , Tamil Nadu ,India

²Associate Professor , Department of Mechanical Engineering , Gnanamani College of Technology ,Namakkal , Tamil Nadu ,India

³Research And Development Head , TejaTech Automation Pvt Ltd , Erode ,Tamilnadu India.

⁴Assistant Professor , Department of Mechanical Engineering , Gnanamani College of Technology ,Namakkal , Tamil Nadu ,India

tejatech2015@gmail.com

Abstract- The purpose of this project is to develop a procedure to numerically model airflow over airfoils using Comsol4.3 Multiphysics. The procedure is to be used as an introduction to numerical analysis tools by take given first NACA[National Advisory Committee for Aeronautics] profiles , Aerodynamics. Two dimensional models for the airfoil were created, drawn and meshed in Comsol4.3 using geometry data gathered by the National Advisory Committee for Aeronautics. Those models were read into Comsol4.3 where flow boundary conditions were applied and the discredited Navier-Stokes equations were solved numerically. The airfoil section lift coefficient from the numeric simulation was compared with Experimental data from the literature and shown to agree within 10% for angles of attack below 10°. Accurate lift coefficients could not be generated for angles of attack greater than 10°. Future concern An attempt was made to demonstrate wingtip vortices from a 3-D model. Unfortunately, due to the inability to develop a reliable mesh this task was one numerical Results take it successfully completed.

keyword : windmill, nano,design , 3dmodel,comsol,airfoil

INTRODUCTION

Flight has been a major part of the world since it was first demonstrated by the Wright brothers in 1902. However, in depth studies into the effects of airflow over wings didn't occur until World War I (Anderson). In an attempt to better understand what made a good wing, the National Advisory Committee for Aeronautics, henceforth referred to as the NACA, was founded. In 1933 the NACA tested 78 airfoil shapes in their wind tunnels with the data being published in Technical Report No. 460, "The Characteristics of 78 Related Airfoil Sections from Tests in the Variable-Density Wind Tunnel." This report also resulted in the creation of the four-digit scheme for defining the basic geometry of the airfoil. This same naming scheme was then used to define the other airfoil families, such as the five-digit airfoils. In 1939 a low-turbulence two-dimensional wind tunnel was constructed for the sole purpose of airfoil testing (U.S. Centennial).

This report outlines the numeric procedure to analyze the NACA airfoil 0012 with a chord length of one meter and the Reynolds numbers of 3x10⁶, 6x10⁶, and 9x10⁶. Both a two and three dimensional model were created to compare FLUENT's accuracy in the two dimensional analysis and an actual sealed wing section three dimensional analysis. The numerical process used for

this airfoil will be used as a tutorial for students taking MAE 4440/7440, Aerodynamics, where they will be required to numerically analyze an airfoil of their own design. Once a procedure to replicate the NACA empirical data was found, an attempt to make a model showing the wingtip vortices phenomenon was constructed.

Unfortunately, a suitable mesh could not be found for the complicated airfoil geometry.

1.1 Four-digit Airfoils

All the airfoils in the NACA four-digit airfoil family are defined by a series of four numerical digits, i.e. 2412. The first digit is the maximum value of the mean line in hundredths of the chord and is represented in the following equations with the letter m. The second number represents the position on the chord of the maximum mean line in tenths of the chord and is represented with the letter p. The last two numbers designate the maximum thickness of the airfoil in hundredths of the chord and is represented by t. Therefore, the airfoil 2412 tells us that the airfoil has a maximum mean line value of two hundredths of the chord length at a position four tenths the chord from the front of the airfoil and a maximum thickness of twelve hundredths the chord length, see figure 1.

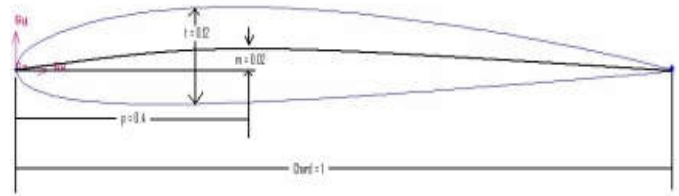


Fig. 1.1 Diagram displaying the chord length, maximum chamber, position of max chamber and max thickness of the airfoil geometry.

The NACA four-digit wing sections are based upon a set of geometric equations which makes this family of airfoils easy to derive by finding a set of coordinates that define the upper and lower

surfaces of the airfoil. These equations will define the coordinates of the

surfaces for a given airfoil as percentages of the chord. When an analysis is to be conducted on an airfoil with a chord lengths not equal to one, the coordinates for the airfoil must first be found for a chord length of one and then multiply the coordinates, both x and y, by the desired chord length. The coordinates for the upper surface can be

found with the following equations:

$$x_u = x - y_t \sin \theta$$

$$y_u = y_c + y_t \cos \theta \tag{1}$$

Likewise the lower surface coordinates can be found using the equations below:

$$x_l = x + y_t \sin \theta$$

$$y_l = y_c - y_t \cos \theta \tag{2}$$

where x is the position along the chord, y_t is the corresponding thickness distribution and θ is the angle between the previous point and the current point. When NACA first began trying to determine the best geometry for wings, they looked at the Clark Y and Göttingen 398 which were two of the most successful wing designs at the time.

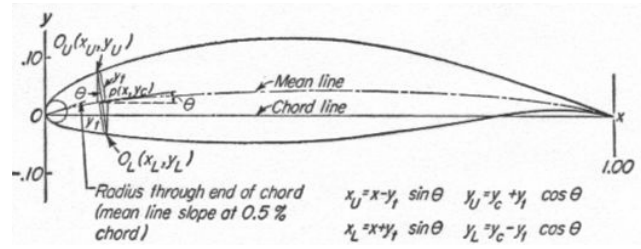
They found that when the chamber was removed, that the effective thickness distribution of the two wings was nearly the same. Therefore, the thickness distribution for the four-digit wing sections was defined off the geometry of those current wing sections and is defined by the equation:

$$\pm y_t = \frac{t}{0.20} (0.29690\sqrt{x} - 0.12600x - 0.35160x^2 + 0.28430x^3 - 0.10150x^4) \tag{3}$$

The leading edge radius of the four-digit airfoils is defined by the equation:

$$r = 1.1019t^2 \tag{4}$$

where the center of the circle this radius defines is located at 0.05 percent of the chord on the mean line, see figure 2.



The chamber of an airfoil is defined by the amount of curve in the mean line. The mean line is defined by two parabolic arcs tangent to the position of the maximum mean-line ordinate. The equations that define the mean line

$$y_c = \frac{m}{p^2} (2px - x^2) \text{ forward of maximum ordinate}$$

$$y_c = \frac{m}{(1-p)^2} [(1-2p) + 2px - x^2] \tag{5}$$

Through the use of equations 1-6 any number of four-digit airfoil coordinates for the upper and lower surfaces can be defined aft of maximum ordinate (6)

1.2 Comsol4.3

Comsol4.3 is a modeling software that is capable of creating meshed geometries that can be read into FLUENT and other analysis software. An outline for the Comsol4.3 geometry creation process can be seen in figure 3.

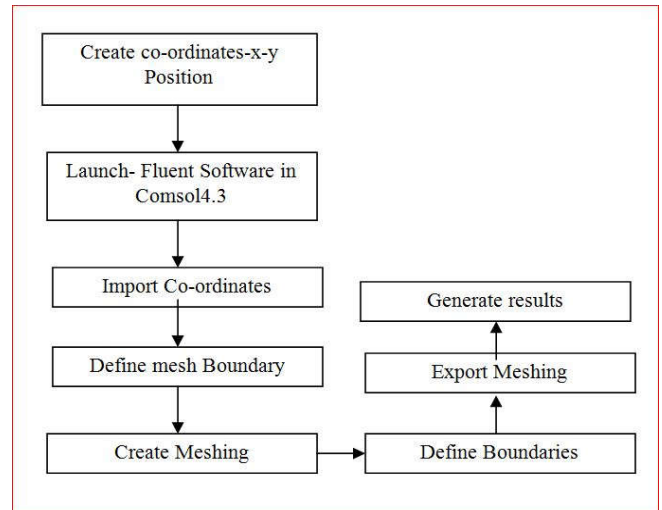


Figure 1.3 Fluent Process

CHAPTER-2

LITERATURE SURVEY

M.O.L. Hansena li at al [1] The aerodynamic part starts with the simple aerodynamic Blade Element Momentum Method and ends with giving a review of the work done applying CFD on wind turbine rotors. In between is explained some methods of intermediate complexity such as vortex and panel methods. Also the different approaches to structural modeling of wind turbines are addressed.

Jang-Oh MO [2] considered Five different inflow velocities, in the range $V_{in} = 7.0-25.1$ m/s, are used for the rotor blade calculations. The calculated power coefficient is about 0.35 at a TSR of 5.41, corresponding to 7 m/s, and showed considerably good agreement with the experimental measurements, to within 0.08%. It was observed that the 3-D stall begins to generate near the blade root at a wind speed of 7 m/s. Therefore, root design approaches considering the appropriate selection of the angle of attack and the thickness are very important in order to generate the stall on the blade root.

V.Parezanovic, B. [3] The main point of this paper is the design of the airfoils that could increase the overall efficiency of wind turbines. Every aerodynamic surface must undergo an expensive process of testing of its performance in a wind tunnel. The objective of this paper will be to show that we can minimize the need for costly experiments by introducing modern information technologies into the design process. Using a commercial fluid dynamics solver such as Fluent, we will calculate the performance of several existing airfoils, which are frequently used in wind turbines.

Dr. S. P. Vendan [4] The aerodynamic profiles of wind turbine blades have crucial influence on aerodynamic efficiency of wind turbine. This involves the selection of a suitable airfoil section for the proposed wind turbine blade. The NACA 63 series is chosen as the basic group for investigation because they have good low speed characteristics and the power curve is better in the low and medium wind speed ranges. In this paper NACA 63-415 airfoil profile is considered for analysis of wind turbine blade. NACA 63-415 airfoil profile is created by using the co-ordinate file generated in JavaFoil.

Naishadh G. [5] The objective behind this research is to develop a fluid-structural interaction (FSI) system for SERI-8 composite blade to maximize aerodynamic efficiency and structural robustness while reducing blade mass and cost. In the previous research, a MDO process of a composite wind turbine blade has been pioneered as effective process to develop structurally optimized blade design.

David D. [6] The effects of modifying the inboard portion of the NREL Phase VI rotor using a thickened, flatback version of the S809 design airfoil are studied using a three-dimensional Reynolds-averaged Navier-Stokes method. The results of this study demonstrate that a thick, flatback blade profile is viable as a bridge to

connect structural requirements with aerodynamic performance in designing future wind turbine rotors.

N. S. Asseff and H. Mahfuz [7] The focus of this work is on the turbine blade design. Much has been learned from the advances in wind turbine blade design, but many differences exist that must be addressed. The media density in our case is seawater, which is 800 times denser than air, leading to much higher working loads. The ocean is also a very corrosive environment, so materials have to be properly selected. Also, most wind turbine blades are hollow to reduce self weight and cost, but this type of design is not practical for an ocean

current turbine blade

R.S. Amano, R.J. Malloy [8] Most blades available for commercial grade wind turbines incorporate a straight span-wise profile and airfoil shaped cross sections. These blades are found to be very efficient at lower wind speeds in comparison to the potential energy that can be extracted. However as the oncoming wind speed increases the efficiency of the blades decreases as they approach a stall point. This paper explores the possibility of increasing the efficiency of the blades at higher wind speeds while maintaining efficiency at the lower wind speeds. The design intends to maintain efficiency at lower wind speeds by selecting the appropriate orientation and size of the airfoil cross sections based on a low oncoming wind speed and given constant rotation rate. The blades will be made more efficient at higher wind speeds by implementing a swept blade profile.

Travis Justin Carrigan [9] The objective is to maximize the torque while enforcing typical wind turbine design constraints such as tip speed ratio, solidity, and blade profile. By fixing the tip speed ratio and solidity of the wind turbine, there exists an airfoil cross-section for which the torque can be maximized, requiring the development of an iterative design system.

A.V.Pradeep [10] The GE 1.5sle MW wind turbine and NREL NASA Phase VI wind turbine have been used as test cases. Details of the design system application are described, and the resulting wind turbine geometry and conditions are compared to the published results of the GE and NREL wind turbines. A 2D wing analysis code XFLR5, is used for to compare results from 2D analysis to blade-to-blade analysis and the 3D CFD analysis. This kind of comparison concludes that, from hub to 25% of the span blade to blade effects or the cascade effect has to be considered, from 25% to 75%, the blade acts as a 2d wing and from 75% to the tip 3D and tip effects have to be taken into account for design considerations. In addition, the benefits of this approach for wind turbine design and future efforts are discussed.

S. RAJAKUMAR [11] In this paper NACA 4420 airfoil profile is considered for analysis of wind turbine blade. The wind turbine blade is modeled and several sections are created from root to tip. The Lift and Drag forces are calculated at different sections for angle of attack from 0o to 12o for low Reynolds number. The analysis showed that angle of attack of 5o has high Lift/ Drag ratio. The CFD analysis is also carried out at various sections of blade at angle of attack of 5o. The pressure and velocity distributions are also plotted. The airfoil NACA 4420 is analyzed based on computational fluid dynamics to identify its suitability for its application on wind turbine blades and good agreement is made between results.

Prof. John P. Sullivan [12] The problem undertaken is the aerodynamic design of a large horizontal-axis wind turbine. To serve as a baseline for comparison purposes, a turbine with established geometry and performance data was found. This turbine was the Mod-2 wind turbine, built by Boeing in the late 1970s. Table 1 gives the geometry and operational data of the turbine.

O. ZLEM CEYHAN[13] An aerodynamic design and optimization tool for wind turbines is developed by using both Blade Element Momentum (BEM) Theory and Genetic Algorithm. Turbine blades are optimized for the maximum power production for a given wind speed, a rotational speed, a number of blades and a blade radius. The optimization variables are taken as a fixed number of sectional airfoil profiles, chord lengths, and twist angles along the blade span. The airfoil profiles and their aerodynamic data are taken from an airfoil database for which experimental lift and drag coefficient data are available. The BEM analysis tool developed is first validated with the experimental data for low wind speeds. A 100 kW wind turbine, which is used in the validation, is then optimized. As a result of the optimization, the power production is improved by 40 to 80 percent. The optimization methodology is then employed to design a 1MW wind turbine with a 25m radius.

Franck Bertagnolio[14] The aim of this work is two-sided. Firstly, experimental results obtained for numerous sets of airfoil measurements are collected and compared with computational results from the 2D Navier-Stokes solver EllipSys2D, as well as results from the panel method code XFOIL. Secondly, we are interested in validating the code EllipSys2D and finding out for which airfoils it does not perform well compared to the experiments, as well as why, when it does so. The airfoils are classified according to the agreement between the numerical results and experimental data. A study correlating the available data and this classification is performed. It is found that transition modelling is to a large extent responsible for the poor quality of the computational results for most of the considered airfoils. The transition model mechanism that leads to these discrepancies is identified. Some advices are given for elaborating future airfoil design processes that would involve the numerical code EllipSys2D in particular, and transition modelling in general.

CHAPTER-3

PROBLEM FINDING

[1] CFD Investigation on the aerodynamic characteristics of a small-sized wind turbine of NREL PHASEVI operating with a stall-regulated method.[1]

□ Five different inflow velocities, in the range $V_{in} = 7.0-25.1$ m/s, are used for the rotor blade calculations. The calculated power coefficient is about 0.35 at a TSR of 5.41, corresponding to 7 m/s, and showed considerably good agreement with the experimental measurements, to within 0.08%.

□ root design approaches considering the appropriate selection of the angle of attack and the thickness are very important in order to generate the stall on the blade root.

□ It was observed that the 3-D stall begins to generate near the blade root at a wind speed of 7 m/s. This is recognized to have a higher angle of attack than the stall angle of attack, and a maximum thickness of 47% of the chord length. Therefore, in the case of a stall-regulated method, it is judged that root design approaches considering the appropriate selection of the angle of attack and the thickness are very important in order to generate the stall on the blade root.

□ Through analysis of existing experimental data, the angle of attack corresponding to the maximum lift-to-drag ratio was found to be in the vicinity of 6° , regardless of the Reynolds number. This fact will assist designers in performing the pitched-controlled or stall-regulated design of a rotor blade. The calculated lift force to drag force ratio for a given Reynolds number and angle of attack were some what low compared with the 2-D experimental data. This is attributed to a limitation of the present fully turbulent models without transition effect.

□ It was confirmed that 3-D stall that has separated from the blade root slowly generates and, as the wind increases, spreads toward the tip. This allows the rated output power to remain constant. This wind turbine system is controlled by a flow phenomenon called a stall-regulated method. The computed torque and power coefficients showed considerably good agreement with the experimental measurements, to within 0.08% at a TSR of 5.41, which corresponds to 7 m/s.

□ Through a clear understanding of aerodynamic characteristics of a small-sized NREL Phase VI wind turbine, it is expected that this useful aerodynamic data will be made available to designers as guidance in designing stall-regulated wind turbine blades in the development phase of small-sized wind turbine systems in the future.

[2] DESIGN OF AIRFOILS FOR WIND TURBINE BLADES

□ The main point of this paper is the design of the airfoils that could increase the overall efficiency of wind turbines.

□ Every aerodynamic surface must undergo an expensive process of testing of its performance in a wind tunnel. The objective of this paper will be to show that we can minimize the need for costly experiments by introducing modern information technologies into the design process.

□ Using a commercial fluid dynamics solver such as Fluent, we will calculate the performance of several existing airfoils, which are frequently used in wind turbines. The simulated conditions will correspond to those found in a typical environment of a working wind turbine.

□ Fluent and Xfoil simulation results will be compared with experimental wind tunnel data.

□ Our goal is to achieve a high level of agreement between our results and experimental data, which will enable us to modify current, or design new airfoils with greater efficiency for use in wind turbines.

□ NACA 63(2)215, FFA-W3-211, A-Airfoil geometries are modelling of the laminar-turbulent transition allowed very good agreement

□ between Fluent results and experimental data for both lift and drag coefficients.

□ Lift (Cl) and pitching moment (Cm) coeff. curves , Drag coefficient curve for NACA63(2)215, FFA-W3-211 , A-Airfoil geometries

□ The simulations of these few airfoils yielded results which are, for the most part, in good agreement with available wind tunnel measurements. In order to accurately simulate flow around airfoils at low Reynolds numbers as in cases investigated here.

□ it is necessary to accurately simulate the effects of boundary level transition from laminar to turbulent conditions.

□ This is not a major setback in cases where the location of transition is known, however, if we are going to modify or design new airfoils, which would be better suited for use on wind turbine blades, we must be able to accurately predict such occurrences.

□ There are several models available, such as the transition model by R. Michel; this, coupled with Fluent's capabilities of using user-defined functions, could be a solution to the problems that transition effects impose.

[3] CFD Analysis of Rotating Two-Bladed Flatback Wind Turbine Rotor

□ The effects of modifying the inboard portion of the NREL Phase VI rotor using a thickened, flatback version of the S809 design airfoil are studied using a three-dimensional Reynolds-averaged Navier-Stokes method.

□ A motivation for using such a thicker airfoil design coupled with a blunt trailing edge is to alleviate structural constraints while reducing blade weight and maintaining the power performance of the rotor.

□ The calculated results for the baseline Phase VI rotor are benchmarked against wind tunnel results obtained at 10, 7, and 5 meters per second. The calculated results for the modified rotor are compared against those of the baseline rotor. The results of this study demonstrate that a thick, flatback blade profile is viable as a bridge to connect structural requirements with aerodynamic performance in designing future wind turbine rotors.

□ baseline configuration and a flatback configuration, are used to study these effects at three different wind speeds.

□ This study shows that using a flatback rotor did reduce the torque compared to the baseline rotor at all wind speeds

□ originally optimized for the NREL Phase VI blade with the S809 airfoil section shape. However, changes in the blade load distribution caused by the thickening of the inboard sections and trailing edges require a new analysis of both the twist and planform specifications

□ results presented here appear to indicate that the higher loading generated by the flatback sections requires more twist in the inboard region of the blade. Another mitigating factor is that thickening the airfoil profile to 40% is very aggressive aerodynamically; a somewhat thinner airfoil may be sufficient to satisfy structural requirements. A final mitigating factor is that given

the 40% maximum thickness, the 10% trailing edge flatback is rather thin. Standish and van Dam [5] previously observed that an airfoil thickness-to-flatback ratio of 2-to-1 may be optimal;

□ A last factor to consider is that designing a flatback rotor does not entail being limited to modifying existing designs. Beyond choosing to use a thicker, flatback profile, other parameters such as twist distribution and profile blending between blade sections will also factor into the design of an optimized flatback rotor.

□ What this study does prove is that a thick, flatback blade profile is viable as a bridge to connect structural requirements with aerodynamic performance in designing future wind turbine rotors.

[4] Blade System Design Studies Volume II: Preliminary Blade Designs and Recommended Test Matrix

□ Blade System Design Study (BSDS) concerning innovations in materials, processes and structural configurations for application to wind turbine blades in the multi-megawatt range.

□ The BSDS Volume I project report addresses issues and constraints identified to scaling conventional blade designs to the megawatt size range, and evaluated candidate materials, manufacturing and design innovations for overcoming and improving large blade economics.

□ The current report (Volume II), presents additional discussion of materials and manufacturing issues for large blades, including a summary of current trends in commercial blade manufacturing.

□ Using preliminary design calculations for a 3.0 MW blade, parametric analyses are performed to quantify the potential benefits in stiffness and decreased gravity loading by replacement of a baseline fiberglass spar with carbon-fiberglass hybrid material. Complete preliminary designs are then presented for 3.0 MW and 5.0 MW blades that incorporate fiberglass-to-carbon transitions at mid-span. Based on analysis of these designs, technical issues are identified and discussed.

□ This report provides an overview of general issues for large wind turbine blades. Current manufacturing trends are summarized, and several design options for incorporating carbon fiber in blades are presented.

□ Preliminary blade designs were developed at 3.0 and 5.0 MW, and parametric analyses were performed to investigate the potential benefits and options for inclusion of carbon fiber in MW-scale blade spars.

□ Critical performance aspects of the carbon material and blade structure are discussed within the context of coupon and sub-structure testing planned for the next phase of this project. Finally, recommendations are made for composites testing under Part II of the BSDS, and the initial planned test matrix for that program is presented.

[5] CFD Analysis Of Wind Turbine Blade .

A wind turbine is a rotary device that extracts energy from the wind. Wind energy has been shown to be one of the most viable sources of renewable energy.

□ [1]. with current technology, the low cost of wind energy is competitive with more conventional sources of energy such as coal. Rotor blade is a key element in a wind turbine generator system to convert wind energy in to mechanical energy.

□ [2]. Most blades available for commercial grade wind turbines incorporate airfoil shaped cross sections. These blades are found to be very efficient at lower wind speeds in comparison to the potential energy that can be extracted.

□ Computational fluid dynamics (CFD) is a branch of fluid mechanics that uses numerical methods and algorithms to solve and analyse problems that involve fluid flows. Computers are used to perform the calculations required to simulate the interaction of liquids and gases with surfaces defined by boundary condition.

□ [3] In this paper, CFD analysis of wind turbine blade, a complete drawing, and details of sub-system are carried out.

□ In this project of CFD analysis of wind turbine blade CAD drawing of the blade is drawn in Pro-E software, meshing is done in COMSOL 4.3 and blade is analyzed in FLUENT CFD software. The following conclusions emerge from this study.

□ It was observed that value of numerical power increases as angle of attack increases from 00 to 70, after 70 the value of numerical power reduced. Hence critical angle of attack for this blade is 70.

□ The maximum value of coefficient of performance (CPmax = 0.271) was observed at angle of attack 70 and at velocity of air 8 m/s.

□ This blade can generate maximum power of 620 W at maximum CP, angle of attack 70 and velocity of air 8 m/s.

□ From the graph Fig. No. 7.1 it was observed that coefficient of performance is increases from 3 m/s to 8 m/s and after 8 m/s value of coefficient of performance reduced.

Objective

- New technique introduce the using modelling flow in high speed external aerodynamic applications.
- airfoil blade shape optimization analysis.
- Transonic flow will be modelled over a NACA 0012 airfoil for which experimental data has been published, so that a comparison can be made.
- Develop design specifications for large blades (1.5 MW to 5.0 MW size range).
- Perform preliminary designs for a megawatt-scale blade, and identify areas of risk that merit testing before proceeding to detailed design.
- Document the project's progress and results in a manner that makes the information readily available to wind industry, composite manufacturers, and other interested parties.
- The current report addresses objectives #1 through #6.

- The solver used is the density based implicit solver, which gives good results for high speed compressible flows.

- The using FLUENT and Ansys CFDPost from within Workbench, but it could also be completed in standalone mode.

Overview

1. Selection of Aerofoils for MW wind turbine (NACA 63(2)215, FFA-W3-211, A-Airfoil, NREL S818, NREL S825, NREL S826 series airfoils family)

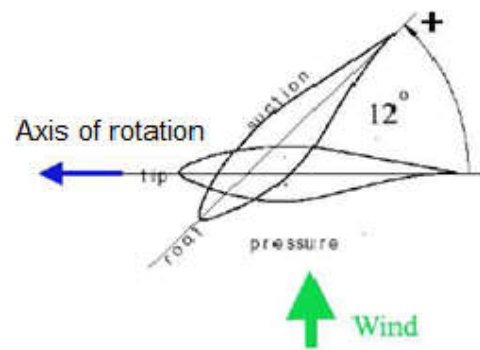
2. Aerodynamic Design: Geometry and Performance

3. Structural Design :Using preliminary design calculations for a 3.0 MW blade, parametric analyses are performed to quantify the potential benefits in stiffness and decreased gravity loading by replacement of a baseline fiberglass spar with carbon-fiberglass hybrid material.

The skins and spar cap are E-glass/epoxy laminate.

□ The triaxial fabric is designated CDB340

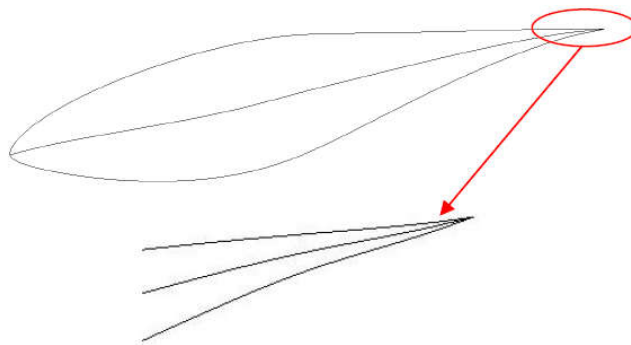
□ The spar cap is composed of alternating layers of triaxial and uniaxial (A260) fabric.



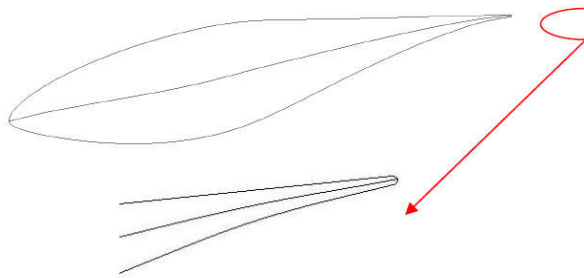
- Cn- spanwise normal force coefficient

- Cp-Pressure coefficient distributions

- This is because the CFD analysis does not model the tower; thus tower wake effects on the blade are not present. Tower effects are slightly noticeable in the experimental upwind data itself, but this is judged to be not significant enough to skew the comparison.



Sharp Trailing edge of the real blade section



Rounded Trailing Edge of the geometric blade section

Figure 3.3: Trailing edge shape

It is believed that, such a change in the trailing edge will not have important effect on the results. Because the results are compared with experimental data. And in experiments, it is not possible to manufacture a blade of very sharp trailing edge.

The geometric blade consists of 4 sections as shown in Figure (3.4);

- Section 1: at the root of the blade
- Section 2: at 30% span where the thickness is reduced to 21%
- Section 3: at midspan
- Section 4: at the tip

CHAPTER-3
METHODOLOGY PROCESS

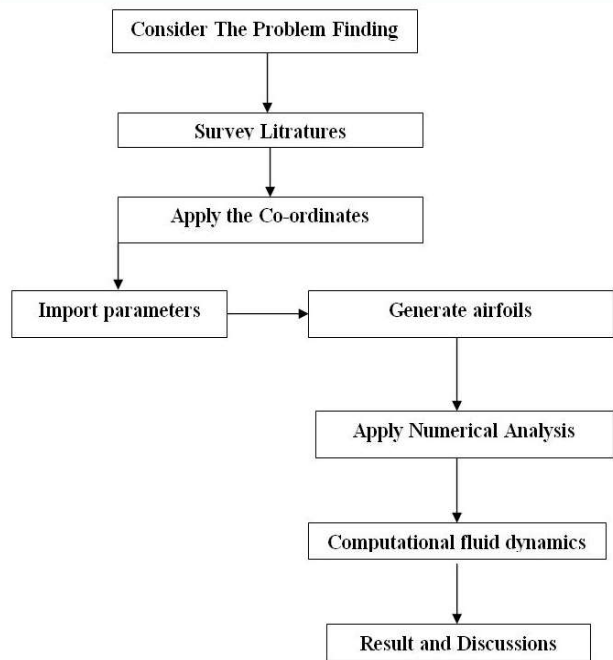


Figure 2.1 Methodology Process

3.1 Apply coordinates

Since the airfoil geometry is defined by sets of coordinate points, the more points defined will increase the accuracy of the model. An airfoil geometry defined by one hundred points for both the top and bottom surface will result in a good definition. The list of coordinates seen in figure 2 were derived by scripting equations 1-6 into a M-file, which can be found in the Appendix, which then supplied the corresponding x, y, and z coordinate for each of the hundred points along the upper and lower surface of the airfoil. With the coordinates defined, they must be listed in a text document in the following format

3.2 Model definition :

Consider the flow relative to a reference frame fixed on a NACA 0012 airfoil with chord-length $c=1.8$ m. The temperature of the ambient air is $20\text{ }^\circ\text{C}$ and the relative free-stream velocity is $U_\infty=50$ m/s resulting in a Mach number of 0.15.

The Reynolds number based on the chord length is roughly $6 \cdot 10^6$, so you can assume that the boundary layers are turbulent over practically the entire airfoil. The airfoil is inclined at an angle α to the oncoming stream.

$$(u_\infty, v_\infty) = U_\infty (\cos \alpha, \sin \alpha) \text{-----} > 1$$

The upstream, top and bottom edges of the computational domain are located 100 chord-lengths away from the trailing edge of the airfoil and the downstream edge is located 200 chord-lengths

away. This is to minimize the effect of the applied boundary conditions.

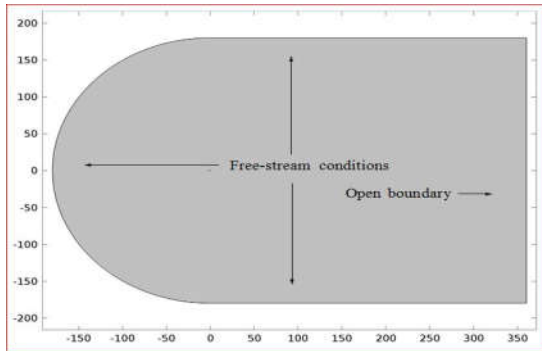


Figure 1.1 shows the flow domain and the applied far-field boundary conditions.

Table 1.1 Proper coordinate format for reading coordinates into Comsol4.3.

| x-coordinate | Y-coordinate | Z-coordinate |
|--------------|--------------|--------------|
| 0 | 0 | 0 |
| 0.0101 | 0.0171 | 0 |
| 0.0202 | 0.0237 | 0 |
| 0.0303 | 0.0285 | 0 |
| 0.0404 | 0.0324 | 0 |
| 0.0505 | 0.0357 | 0 |
| 0.0606 | 0.0385 | 0 |
| 0.0707 | 0.0410 | 0 |
| 0.0808 | 0.0432 | 0 |
| 0.0909 | 0.0452 | 0 |
| 0.1010 | 0.0470 | 0 |
| 0.1111 | 0.0486 | 0 |
| 0.1212 | 0.0500 | 0 |
| 0.1313 | 0.0514 | 0 |

The top two numbers, 100 and 2, tell Comsol4.3 that it is going to read in two sets of one hundred coordinates one right after the other. The column on the left is the x- coordinates. The central column is the y-coordinates and the right column is the z- coordinates. There must be no empty lines between the rows of coordinates and at least one space separating the columns of coordinates from one another. The coordinates should also be listed vertically moving from the nose

of the airfoil toward the tail for the upper surface first and then the lower surface. A note of interest, by using equations 1-6, the two coordinates that define the tail of the airfoil do not bring the geometry to a single point, see figure 5.

| | | |
|--------|---------|---|
| 0.9798 | 0.0041 | 0 |
| 0.9899 | 0.0027 | 0 |
| 1.0000 | 0.0013 | 0 |
| 0 | 0 | 0 |
| 0.9798 | -0.0041 | 0 |
| 0.9899 | -0.0027 | 0 |
| 1.0000 | -0.0013 | 0 |

Fig. 1.2 Airfoil tail gap created by equations 1-6.

This minor gap in the tail of the airfoil is useful when 3-D geometries are being defined in Comsol4.3 so the gap will be maintained. Once properly formatted the document should be saved as a *.txt document.

GENERATIVE AIRFOIL

4.1 Creating the Airfoil Geometry

Launch Comsol 4.3. Once Comsol 4.3 is open make certain the solver is set for the appropriate output, i.e. FLUENT 5/6, by selecting Solver → FLUENT 5/6. The coordinate document must now be imported into Comsol 4.3. This is done by selecting File → Import → Parameter Inputs...

This will open the COMSOL 4.3 import window. Make certain the edge command is selected and that the face command is deselected, as can be seen in figure 7. Once the desired coordinate file to be imported is listed in the File Name text box, accept the settings. Since the text file told Comsol 4.3 to read in two sets of one hundred coordinates, each set of one hundred coordinates will be defined by one edge resulting in Comsol 4.3 window now displaying the upper and lower surface of the airfoil.

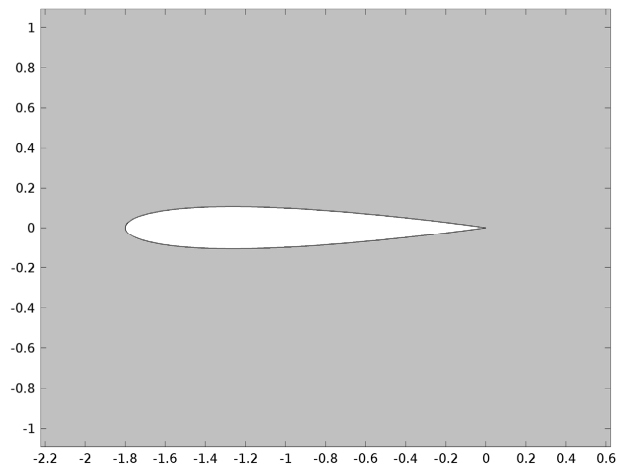


Fig. 4.1 Imported airfoil geometry.

Next the upper and lower surface of the airfoil must be split at three tenths of the chord length since the first thirty percent of the airfoil will be meshed with a non-uniform grid and the last seventy percent of the airfoil with a uniform grid. This is done by selecting the Geometry Command under operation → Edge Command → Split/merge Edges. Start by selecting the upper surface of the airfoil. This edge can either be selected from the popup menu by selecting the up arrow next to the edge box or by shift left-clicking the desired edge. Since Comsol 4.3 created the two current edges in existence they will be represented by the random names edge.1 and edge.2. The first surface imported is defined as edge.1, which is the upper surface, and edge.2 is the lower surface. Also, anytime an entity is selected in Comsol 4.3 that part of the model will be displayed in a different color. Once the edge is selected, enter a value of 0.3c, where c is the chord

length, for the global x-coordinate. This will place a marker on the edge where the split is going to occur. This process can be seen for a 0012 airfoil in the Repeat this process for the lower surface.

4.2 Creating Mesh Boundary

The outer mesh geometry must now be created. This is done by selecting the Vertex Command button under the Geometry Operation. By selecting the Create Vertex button another window with both global and local coordinate options is opened, see Using the global coordinates, it is possible to create the outline for a C-mesh profile around the airfoil geometry. This will allow for a good quick mesh to be created. By filling in the global coordinate positions with the values in Table 1, the outline of the mesh boundary will be defined by nine vertices. Naming all geometries created is highly recommended to ease the process of finding points later in the popup menu.

Table 1.3 Global coordinates of vertices to create outer boundary of mesh where c is the chord length of the airfoil. All plotted points can be seen in figure 11.

| Lab | x- | y- | z- |
|-----|--------|----|----|
| A | c | 9 | 0 |
| B | 14.4*c | 9 | 0 |
| C | 14.4*c | U | 0 |
| D | 14.4*c | 0 | 0 |
| E | 14.4*c | L | 0 |
| F | 14 | - | 0 |
| G | C | - | 0 |
| H | C | 0 | 0 |
| I | - | 0 | 0 |

The y-coordinates UT and LT correspond to the y-coordinates for the upper and lower surface tails of the airfoil, refer to figures 5 and 11. These values are easiest found by

referring to the airfoil coordinate text file. Once these vertices have been created the work frame should appear as follows:

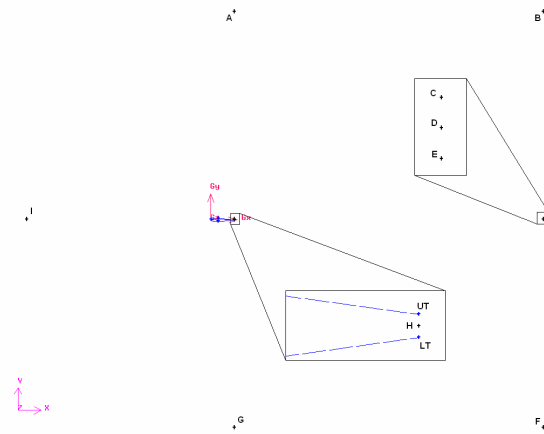
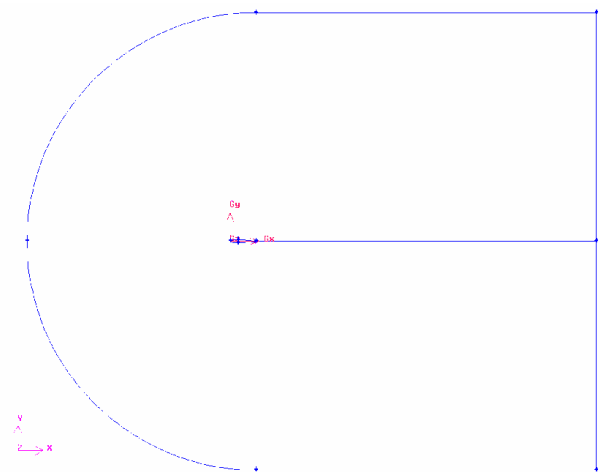


Fig. 1.5 Resulting vertices locations.

This disconnected tail is important for the process in which 3D geometries are created in Comsol 4.3 so don't have the airfoil come to a point at the tail. These vertices must now be connected to create a frame for the faces that are to be meshed. For a face to be created later, all the faces must be completely enclosed. Start by selecting the Geometry Operation → Edge Command → Create Edge Command. The create edge command must be set to create a straight edge. Now select two vertices between which an edge needs to be created. Straight edges need to be created between all of the following point pairs: AB, BC, CD, DE, EF, FG, GLT, LTH, HUT, UTA and DH, as can be seen in figure 12.

The end points are going to be A and I and G and I. The final mesh outer boundary should appear as follows:



Each enclosed area will now be turned into a face which can be meshed. Start by selecting Geometry Operations → Face Command → Form Face Wireframe. In total there will be four faces created. From figure 15 the top right rectangle will be face ABCDH. The

lower right rectangle will be face DEFGH and the left half circle will be face AIGH. The last face will be the area of the airfoil. The first face mentioned is created by picking the edges AB, BC, CD, DH, HUT, and UTA, see figure 16.

The second rectangular face is created with the edges DE, EF, FG, GLT, LTH, and HD. The airfoil is made into a face by selecting the imported edges, these most likely have the generic names edge.1, edge.2, edge.3, and edge.4, and the edges HUT and LTH. The final face is created by selecting the edges UTA, AI, GI, GLT, LTH, and HUT. In order to save processing time the airfoil face doesn't need to be meshed. Therefore, the airfoil can be subtracted from the half circle face AIGH by selecting Geometry Operation → Face Command → right click Boolean Operation → Subtract, see figure 17.

In the upper Face box select the half circle face AIGH. In the Subtract Face box select the airfoil face and then select apply. Do not select the retain options or else multiple edges will exist on top of each other. (For a 3D airfoil analyses go to section 3.5 at this point.)

4.3 Meshing 2D

The process to mesh the faces can now begin. Since the area of interest is around the airfoil, this is the region that the mesh should be the densest.

Start by selecting Mesh Operation → Edge Command → Mesh Edge. This will allow the defining of the face mesh through defined edge meshes. To mesh an edge, select the edge by either the popup menu or by shift left-clicking the edge. Start by selecting edge AB, making certain the arrow is pointing from left to right, see figure 18.

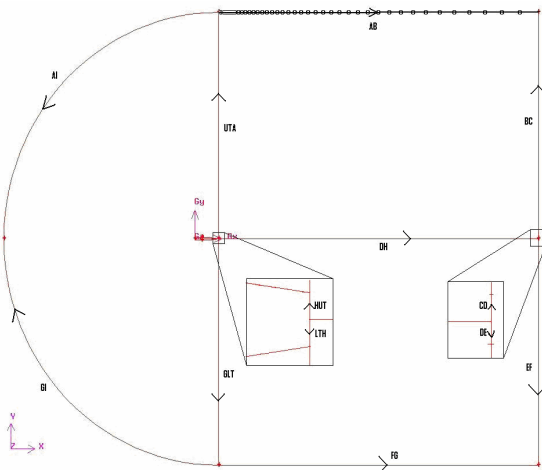


Fig. 1.9 Edge mesh labels and arrow indication.

The arrow direction can be changed by selecting Reverse at the top of the edge mesh window. For this edge, a First Length type mesh is desired, see figure 19. This will place more elements closer to the tail of the airfoil, which is an area of interest, and fewer

elements to the far right where the flow will once again be uniform. Set Length to 0.1 and the Interval Count option in the space box to forty for the initial mesh, see When deciding on the density of the mesh, weigh the cost and benefits of calculation time versus accuracy. Starting out with a less dense mesh is usually best since the density can always be increased in FLUENT and this will reduce calculation times for preliminary results. This process will be repeated for edges DH and FG, again with the arrow pointing from left to right.

The vertical edges UTA, BC, EF, and GLT will be meshed with a Successive Ratio of ratio 1.15 and an Interval Count of 30, refer to figure 19 for edges. Edges UTA and BC should have their arrows pointing up and edges GLT and EF with their arrows pointing down in order to place the densest mesh around the airfoil. The small edges LTH, HUT, CD, and DE will all be meshed with a Successive Ratio of ratio 1 and an Interval Size

of 0.02c with their arrows pointing away from the center. There won't be any notable change along these small edges. Due to the earlier line split conducted on the top and bottom surfaces, the airfoil geometry is now represented by four separate lines. When these edges are meshed their arrows should point towards the tail of the airfoil, see figure 20.



Fig. 1.10 Airfoil arrow direction.

The front edges of the airfoil will be meshed with a Last Length type at a Length of 0.02c, where c is the chord length, and Interval Count of forty. The rear edges of the airfoil will be meshed with a Successive Ratio of one and Interval Size of 0.02c. These small intervals will create a dense mesh right around the airfoil geometry. To determine the number of mesh elements on the rear edges of the airfoil select Mesh Operation → Edge Command → Summarize Edge Meshes and choose either the upper or lower rear edge. Select the elements option and click apply. The number of elements on the line will be printed in the Comsol 4.3 .

Knowing the number of elements on the top and bottom surfaces of the airfoil, an edge mesh can now be generated for the arcs AI and GI with their arrows pointing toward vertex I, see figures 18. These lines will be meshed with a First Length type mesh, Length 0.02c with an Interval Count equivalent to the number of elements on the corresponding top and bottom surfaces of the wing section geometry. The interval count for the 0012 airfoil in this procedure is 75. See figure 22 for a view of all the meshed edges.

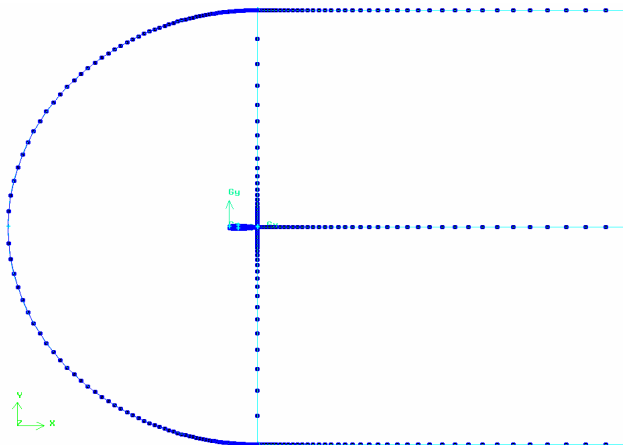


Fig.1.11 All edges meshed.

CD, DE, EF, FG, GI, and AI, refer to figure 18. This boundary condition will be labeled farfield. The last entity that must be defined is the air flow region. This is done by selecting Zone Operation → Continuum Type. The type will be fluid and all three faces should be selected for entity. This continuum will be called air, The mesh can now be exported to a format FLUENT can read. This is done by selecting

File → Export → Mesh. This opens the export window, see figure 26.

Make certain the export 2-D mesh option is selected and that the mesh file is going where desired by checking with the browse button. Then select accept and the 2D mesh is ready to be read into FLUENT.

The faces can now be meshed by selecting the Mesh Operation → Mesh Face Command → Mesh Face. All the faces can be meshed at once by selecting the three previously defined face geometries from the popup window or shift left-clicking the face's edges. The elements option should be set to Quad, type to Map, and smoother to None. All other default values can be kept and the apply button selected. The completed face mesh can be seen in figure 23. (For 3D models go to section 3.6 to continue.)

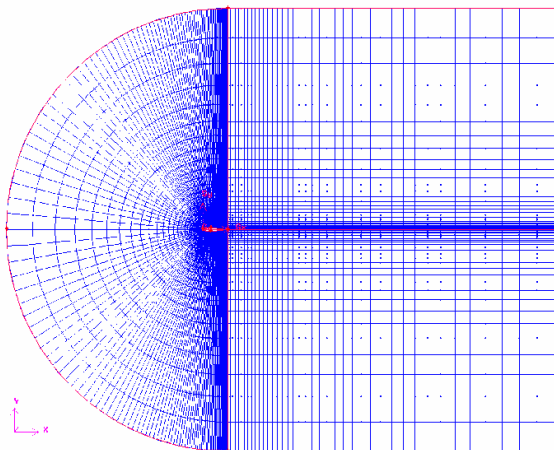


Figure 1.12 Completed Mesh.

The boundary types can now be defined since the meshing is complete. This is done by selecting Zone Operation → Specify Boundary Types. The type option is automatically set to Wall so define the airfoil's boundary first. The entity option should be set to Edges and then select all six edges that define the airfoil geometry, see figure-24. It is a good idea to give all zones and boundary conditions useful names so when imported into FLUENT locating the desired zones will be easier. For this procedure the airfoil boundary will be named airfoil. Next, the type needs to be changed to Pressure-far-field. The edges that make up this boundary condition are all the outer edges of the mesh. This consists of edges AB, BC,

4.4 Creating 3D Wing

This section continues from the end of section 3.3. In order to create the wing section the three faces that were previously created have to be extruded. This is done by selecting Geometry Operation → Volume Command → right-click Form Volume → Sweep Face.

The extrusion will consist of extruding all the faces in the positive z-direction by a magnitude of one. Select the faces through either shift left-clicking them or else through the popup window. The extrusion path will be via a vector so select the vector path option. To change the magnitude of the extrusion click the define button under path and set the magnitude to the desired value. Leave the value at one in the positive z-direction for this procedure, see figure 27.

Swept volumes can be labeled if they are extruded separately. Once the vector magnitude and direction are set click apply to extrude the faces. At this point a large number of faces will have been created with generic labels since volumes are defined by faces which Comsol 4.3 has created through the sweeping process. The easiest method to select a desired face is to continually shift left-click an edge of the face until the desired face is highlighted and then through the popup window remove the faces that should not have been selected. The 3D wing geometry is now created and a mesh for the volumes can be created.

4.5 Meshing 3D

All the faces that existed in the 2D mesh process and their replicas will be meshed in the same fashion as described in section 3.4. Therefore refer to section 3.4 for the face meshing of the 3D geometry. Refer to figure 28 for what a face meshed geometry should look like at the completion of section 3.4. For each volume two opposite faces should now be identically meshed.

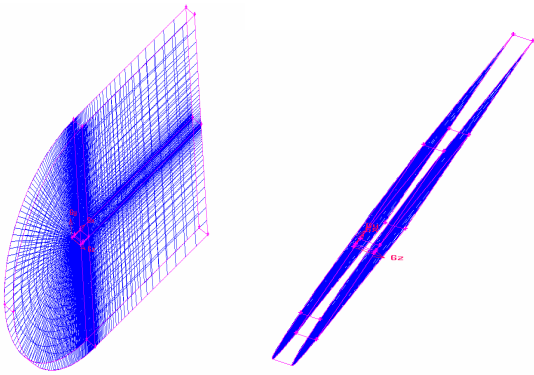


Figure 1.13 All faces and their replica's that were present in section 3.4 are meshed.

In order to mesh the volumes a Cooper mesh will be used. This is done by selecting Mesh Operation → Volume Command → Mesh Volume. This opens the volume mesh window. The volume mesh will be a hex element mesh and type Cooper. The Cooper mesh will take two faces pre-meshed faces, the Sources, and then replicate the mesh on those faces at a desired interval spacing for the volume between the faces. The Cooper mesh will not work trying to mesh along a single line connecting two points of any one volume together. This is why the gap at the end of the airfoil is necessary. Also, for the Cooper mesh to succeed, both of the end faces must be identical. The settings used for the volume mesh in this procedure are seen in figure 29. Thus, using the Cooper mesh process, mesh all the volumes. The spacing value will determine the density of the volume's mesh. The spacing value will be 0.1 for this procedure. The smaller the spacing value the denser the mesh. Remember that while a denser mesh gives better results, the computation time is also increased. Now the boundary conditions for the wing section can be created. This is done by selecting Zone Operation → Specify Boundary Type. Since the boundary type of wall is default the wing's surfaces can be defined first, see figure 30. Don't forget the two thin faces at the tail of the wing section.

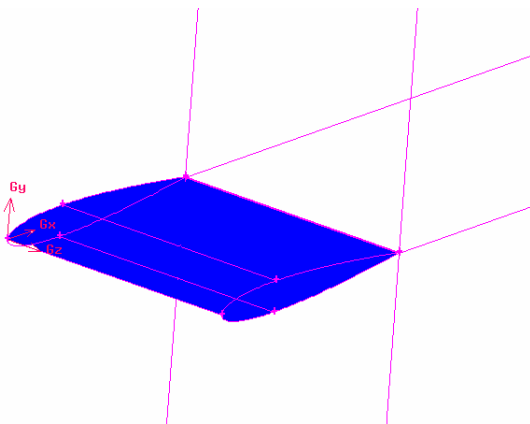


Figure 1.14. The faces that define the wing section.

The wing section is the non-meshed portion of the volume and is defined by six face entities. The next boundary to define is the outer vertical faces that will be defined as symmetry, see figure 31. This will prevent flow distortions along the edges of the volume.

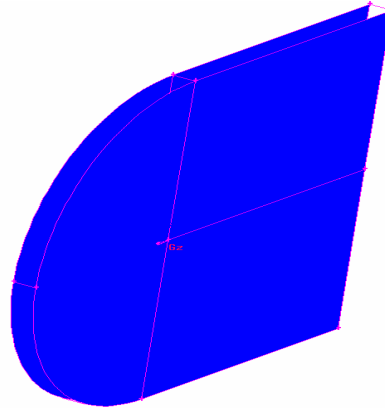


Fig. 1.15 Faces to be defined as symmetry.

The last boundary layer will be defined as a pressure-far-field. There will be eight faces as part of this zone, see figure 32. Don't forget the two small faces in the middle back of the mesh volumes.

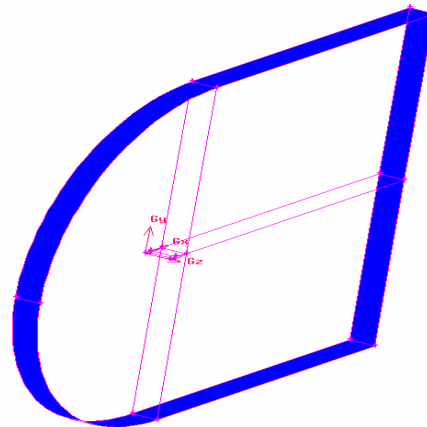


Figure 1.16 Faces to be defined as pressure-far-field.

The final zone that must be defined is the fluid volume. This is done by selecting Zone Operation → Specify Continuum Type. The entity is all the volumes and they will be defined as a fluid type and named air. The 3D geometry is now ready to be exported into a mesh file. This is done by selecting File → Export → Mesh, see figure 26. Make certain the export 2-D(X-Y) mesh option is not selected.

4. FLUENT Procedure

The desired mesh can now be read into FLUENT which will then run the geometry through the numerical analysis. Open FLUENT and select the 2D double precision

operation (2ddp) for two dimensional operations and 3D double precision (3ddp) for three dimensional operations. The Comsol 4.3 mesh is read into FLUENT by selecting File → Read → Case and selecting the appropriate mesh file. Make certain the FLUENT window doesn't display any error messages after reading in the mesh file. First the mesh should be checked by selecting Grid → Check. This will conduct a thorough check of the mesh to make certain no errors are present. The solver to be used on the geometry can be changed by going to Define → Models → Solver. For this analysis a segregated solver will be used so make certain that option is selected. Next, the viscous model must be set by selecting Define → Models → Viscous. Two different viscosity models were tested. The first is the inviscid model which assumes no viscosity. The second is the Spalart-Allmaras (SA) model which is a turbulent eddy viscosity model. Instead of solving for the kinetic energy of turbulence the Spalart-Allmaras model solves directly for the eddy viscosity from a transport equation. The Spalart-Allmaras model was designed for aerospace applications involving wall-bounded flows. After running both viscosity models over a range of angles of attack of 0-20° the results concluded that the inviscid model gave a greater accuracy. Therefore, select the viscous model of inviscid. The following procedure is the same for both the inviscid and Spalart-Allmaras.

Maintain all default values and close the window. The fluid material that is to be used in this analysis is air and the fluid properties can be set by selecting Define → Materials. Air should be the default setting. The density of the air should be changed from constant to ideal gas and viscosity (applies only for SA model) should be changed to the Sutherland three coefficient equation. The default Sutherland values should be maintained. By changing these two properties the density and viscosity will now be

dependent on the temperature of the fluid. Because temperature needs to be monitored now, FLUENT will automatically turn on the energy equation. With these values set click Change/Create and close the materials window. The operating conditions need to be set next. This is done by selecting Define → Operating Condition. This opens a new window where the operating pressure can be set. The operating pressure should be kept at the default standard atmospheric pressure. The next step is to set the boundary conditions for the boundaries that were defined in Comsol 4.3. This is done by selecting Define → Boundary Conditions. The only boundary condition that needs to be modified is the pressure-far-field condition. By selecting farfield, which is the name that was given to this boundary zone in Comsol 4.3, under the zone menu and then click the set button. This brings up the pressure-far-field window. For a Reynolds number of 3×10^6 the Mach number should be set to 0.1261, for a Reynolds number of 6×10^6 the Mach number should be set to 0.2522, and for a Reynolds number of 9×10^6 the Mach number should be set to 0.3783, as seen in figure 33. These Mach number values were found using the Reynolds equation, Eq. 7, for a flat plate to find the free stream flow velocity.

$$Re = \frac{\rho V_{\infty} c}{\mu} \quad (7)$$

with an assumed density, ρ , of 1.225 kg/m³, viscosity, μ , of 1.789×10^{-5} kg/m*s, and the chord length, c , of one and V_{∞} is the free stream velocity. The Mach number is then found with the equation:

$$M = \frac{V_{\infty}}{a_{\infty}}$$

where M is the Mach number and a_{∞} is the speed of sound equal to 347.51 m/s at standard temperature and pressure.

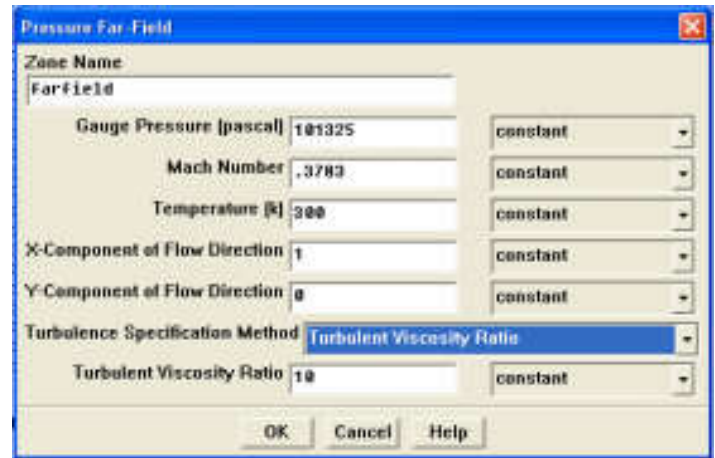


Fig. 33. Pressure-far-field window setup.

The flow directions will be adjusted to account for the angle of attack. If the angle of attack is 10° then the x-component would be the $\cos(10^\circ) = 0.9848$ and the y-component would be the $\sin(10^\circ) = 0.17365$. For a 3D model a z-component flow direction can be set, however, for the 3D procedure conducted here the z-component will remain zero.

For external flows the turbulent viscosity ratio should be set between 1 and 10 so the default value of ten will be kept. The solution controls can now be set. This is done by first selecting Solve → Control → Solution... The solution relaxation for each parameter can be changed in this window. Generally the only time these relaxation parameters need to be changed is if repetitive oscillations begins to occur on the coefficient of lift and drag plots.

The discretization schemes can be modified. Start by changing the pressure discretization value to Presto and leave all the other values set to their default settings. Selecting more complicated discretization schemes, such as second order upwind and power law, will affect the calculation time and convergence stability. Next the solver must be initialized by selecting Solve → Initialize → Initialize... In the compute from dropdown list choose farfield.

This will automatically insert values into all the remaining text boxes in this window. These values should correspond to the farfield boundary settings. Select init and then close. Next the convergence criteria needs to be set. This is done by selecting Solve → Monitors → Residual... In the upper left corner of the new window are the options to print and plot the current convergence criteria values. Since we only care that the model converges and not the exact values at which the convergence occurs select the plot option and deselect the print option. This will keep the main FLUENT window from cluttering with an abundant amount of information.

The minimum convergence criterion should be set to 1×10^{-6} for each residual. Due to the large number of cells in 3D models a small convergence criterion can lead to long computation times. In order to directly monitor the lift coefficient being experienced by the airfoil, select Solve → Monitor → Force... With the force monitors window open select lift for the coefficient to be monitored. Under options check the print and plot boxes and for wall zones select the airfoil profile. The force vectors have to be set to correspond to the angle of attack for which the model is going to be calculated.

This means for an angle of attack of 10° the x force vector should have a value of –

$\sin(10^\circ) = -0.17365$ and a y force vector of $\cos(10^\circ) = 0.9848$, see figure 18.



Fig. 34. Force Monitors window set to monitor the lift coefficient for an angle of attack of 10° .

The drag coefficient can be monitored in a similar fashion but accurate results for the drag coefficient weren't found. Next the reference values must be set. All force monitor calculations for the model will use these values. Select Report → Reference Values... In the compute from dropdown menu select farfield and for reference zone select the fluid zone that was defined in Comsol 4.3, air. While this will set most of the reference values correctly, the actual dimensions of the airfoil geometry have to be set-independently. Since the chord length of this procedure is one meter and the depth is one meter, the default values are correct. Now the model is ready to be solved. This is done by selecting Solve → Iterate... Since convergence criteria were defined, the number of iterations chosen should be relatively large to make certain a solution has time to converge. The number of iterations will be set to 10,000. The other values in this window will be left at their default values. Begin the iteration process by selecting iterate. Once the model finishes iterating the accuracy of the results should be checked. A number of four-digit airfoils have already had coefficient of lift plots generated from NACA empirical data. These plots can be found in many different sources. For this procedure the values will be compared to figures 35, 36, and 37 in section 5.2 from reference 1. If the results are not within a range of accuracy desired several steps can be taken to try and improve the solution. The first, is to change the discretization values under the Solve → Control → Solution... window. The second is to increase the

density of the mesh, through the adapt command, or reduces the convergence criteria. No improvements were found do to convergence criteria less than 10^{-10} . Table 2 gives the settings with which the best solutions were found for the 0012 inviscid model.

Table 2. Setting discretization and mesh adaptation settings for 0012 inviscid model for best results.

| Mach: 0.1261 | | | |
|--------------|-----------|-----------|-------|
| AoA | Density | Momentum | Adapt |
| 0 | 1st Order | 1st Order | None |
| 4 | 2nd Order | 2nd Order | None |
| 8 | 2nd Order | Power | 7436 |
| 12 | 2nd Order | Power | None |
| 16 | 2nd Order | Power | None |
| 20 | 2nd Order | Power | None |
| Mach: 0.2522 | | | |
| AoA | Density | Momentum | Adapt |
| 0 | 1st Order | 1st Order | None |
| 4 | 2nd Order | 2nd Order | None |
| 8 | 2nd Order | Power | None |
| 12 | 2nd Order | Power | None |
| 16 | 2nd Order | Power | None |
| 20 | 2nd Order | Power | None |
| Mach: 0.3783 | | | |
| AoA | Density | Momentum | Adapt |
| 0 | 1st Order | 1st Order | None |
| 4 | 2nd Order | 2nd Order | None |
| 8 | 2nd Order | Power | None |
| 12 | 2nd Order | Power | None |
| 16 | 2nd Order | Power | None |
| 20 | 2nd Order | Power | None |

To increase the accuracy of the model by increasing the number of cells that exist around the airfoils surface select Adapt → Boundary... Adapting the cells around the boundary of the airfoil geometry will break each of the boundary cells into four cells resulting in a denser mesh. However, by increasing the density of the mesh the calculation time is increased. Under boundary zones select the airfoil geometry and click the mark button.

A note will popup in the main FLUENT window indicating the number of cells to be adapted. To adapt these cells simply click the adapt button in the boundary adapt window and select ok in the adapt warning window. After the adapt process is complete

the main FLUENT window will print out the results of the adapting process.

The number under the adapted column indicates the current number of cells in the mesh. The 7436 in

Table 2 under adapt is referring to this value. Now that the mesh is denser the model must be reinitialize and then the iteration process repeated.

5.3 Wingtip Vortices Model

A three dimensional wing model was created using the same process described in section

3.5. The only addition was a second volume extrusion in the positive z-direction, see figure 25.

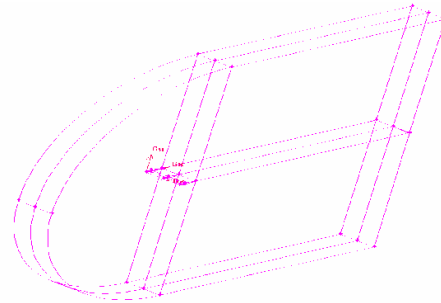


Fig. 38. Extruded Wing model.

An attempt was then made to mesh half of the wing section as a fluid to create the conditions necessary for a wingtip vortex to occur. However, due to the airfoils peculiar geometry a quad mesh was not possible. A tri mesh on the two end faces of the airfoil was attempted so that a Cooper mesh could be performed for the volume. Unfortunately, the face's meshes did not come out identical, see figure 26.

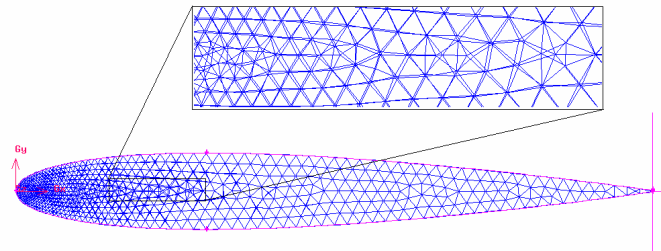


Fig. 39. Displaying the failure of the Tri pave mesh.

The reason for this is unknown since both geometries were identical. The only face mesh that resulted in identical faces was a Quad/Tri map. Unfortunately, this results in an extremely skewed mesh which led to inaccuracy in the results, see figure 27.

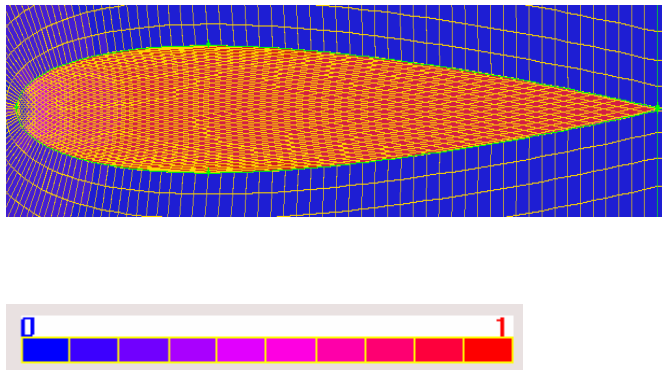


Fig. 40. Displaying the Quad/Tri map mesh generated for the meshed wing section. Resulted in skewed cells which give poor results.

An attempt was made to use FLUENT to analyze the mesh with the skewed cells, however, due to the skewed cells no convergence ever occurred. After 5000 iterations the model was stopped and an attempt was made to see if any wingtip vortex was discernable. This attempt resulted in the computer running out of memory and no final visual representation of the model could be plotted. While it is likely FLUENT is capable of modeling wingtip vortices, an alternate mesh method will have to be attempted and a more powerful computer may be necessary to solve the model.

RESULT AND DISCUSSION

Comparison of 2-D Numerical Results to NACA Empirical Data

Through conducting this research, a process to obtain results with less than a 10% error, when compared to NACA empirical data, using FLUENT, was found for angles of attack less than 10°. However, as the angle of attack of the airfoil increased beyond 10° the accuracy also decreased. Figure 35, 36, and 37 show a comparison of the FLUENT produced results as compared to the NACA empirical data as well as the accuracy at a given angle of attack for the Reynolds numbers of 3x10⁶, 6x10⁶, and 9x10⁶ respectively.

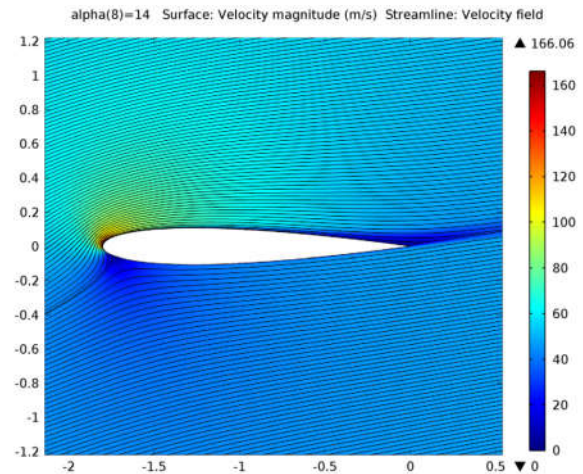


Figure 3: Velocity magnitude and streamlines for the flow around a NACA airfoil.

Figure shows the velocity magnitude and the streamlines for the steady flow around the NACA 0012 profile at $\alpha=14^\circ$. A small separation bubble appears at the trailing edge for higher values of α and the flow is unlikely to remain steady and two-dimensional hereon. Provides experimental data for the lift coefficient versus the angle of attack. Values have been plotted for both the inviscid and Spalart-Allmaras model.

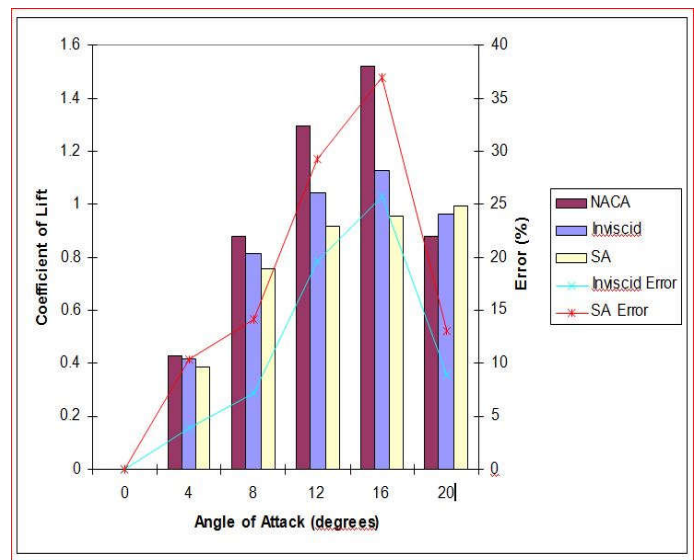


Fig. 35. Plot of coefficient of lifts versus NACA empirical data and percent error difference between the results for Reynolds number 3x10⁶.

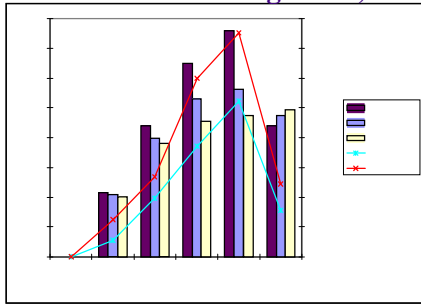


Fig. 36. Plot of coefficient of lifts versus NACA empirical data and percent error difference between the results for Reynolds number 6×10^6 .

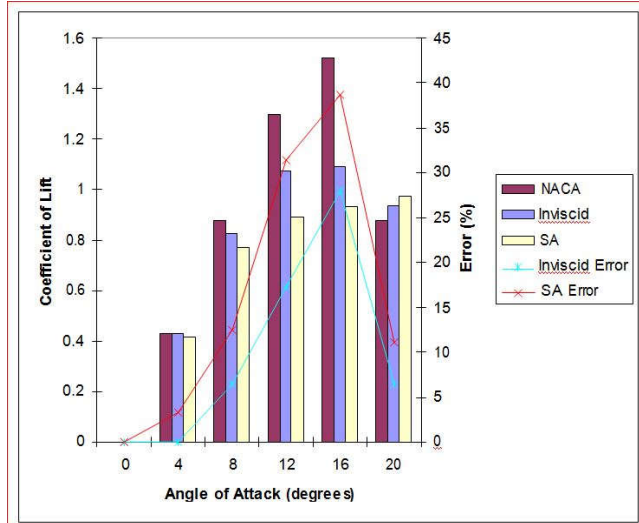


Fig. 37. . Plot of coefficient of lifts versus NACA empirical data and percent error difference between the results for Reynolds number 9×10^6 .

As can be noticed from these figures, the inviscid model produced more accurate results at every angle of attack. Also, the accuracy of either model doesn't necessarily increase or decrease corresponding to the flow velocity. As the angle of attack increases the accuracy of both models drops dramatically. Attempts to increase this accuracy were made by both increasing the density of the mesh and the tightening the convergence criterion. Unfortunately, neither reducing the convergence criterion less than 10-10 nor increasing the density of the mesh resulted in an increase of accuracy for the lift coefficient. This large error could be due to the fact that statistical (Reynolds averaged Navier-Stokes) turbulence models have difficulty solving problems with large eddy turbulence effects (Mellen). Thus, using FLUENT's inviscid model, lift coefficients can be found within 10% of their empirical values for angles of attack less than 10° .

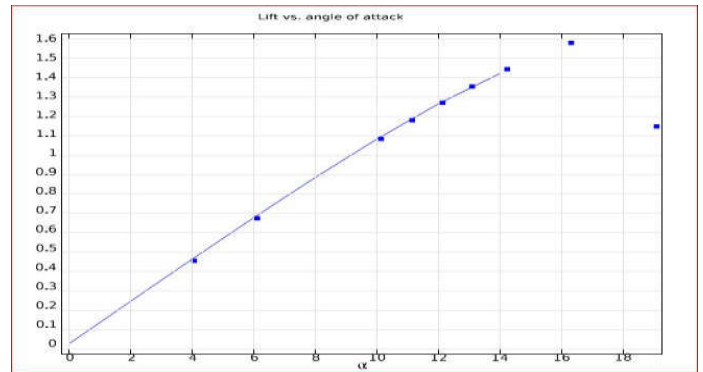


Figure 4: Computational (solid) and experimental (dots) results for the lift coefficient vs. angle of attack.

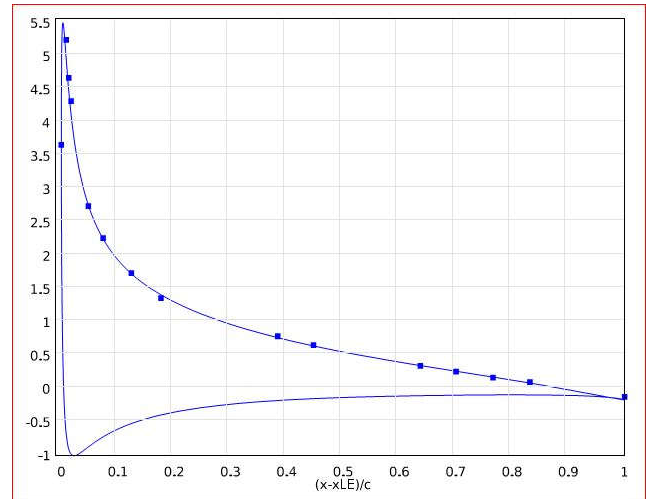


Figure 5: Computational (solid) and experimental (dots) results for the pressure coefficient along the airfoil.

CONCLUSION

By following the procedure as described above, both a 2-D airfoil design in NACA profile its simulated in Fluent Software and The performance achieved conserve 3-D model of the four- digit airfoil 0012 were created and meshed .When these models were run in FLUENT under the same conditions identical results were produced. This goes to prove the validity of using a simpler 2-D model for analyzing airflow over airfoils instead of the more time consumed computational fluid experimentally analysed in results are compared in reynolds Number ,Lift co-efficient ,Thrust Velocity are results are done it.

FUTURE SCOPE :

In our future scope its concerned The techniques to be applying in more airfoils consist while achieved the performance basis . After the survey of CFD measurement to equally constructing the airfoil have generate in turbine model in three dimensionally simulating computational fluid dynamics. Finally in our research

consister structured model analysis to finalized vibration effective also simulated and compare with other models in research goal.

Reference:

1. M.O.L. Hansena, J.N. Sorensena, S. Voutsinasb, N. Sorensenc,d, H.Aa. Madsenc, State Of The Art In Wind Turbine Aerodynamics And Aeroelasticity, Elsevier, 29-Dec-2006.
2. Jang-Oh MO1 and Young-Ho LEE2, Cfd Investigation On The Aerodynamic Characteristics Of A Small-Sized WindTurbine Of Nrel Phase Vi Operating With A Stall-Regulated Method, oct-12, 2011.
3. V.Parezanovic, B. Rasuo, M. Adzic, Design Of Airfoils For Wind Turbine Blades.
4. Dr. S. P. Vendan1, S. Aravind Lovelin2, M. Manibharathi2 and C. Rajkumar2 , Analysis of a Wind Turbine Blade Profile for Tapping Wind Power at the Regions of Low Wind Speed, Ijmejournal.
5. Naishadh G. Vasjaliya1 and Sathya N. Gangadharan, Aero-Structural Design Optimization of Composite Wind Turbine Blade.
6. David D. Chao and C.P. "Case" van Dam, CFD Analysis of Rotating Two-Bladed Flatback Wind Turbine Rotor , SANDIAREPORT /April-2008.
7. N. S. Asseff and H. Mahfuz, Design and Finite Element Analysis of an Ocean Current Turbine Blade, Feb-2009.
8. R.S. Amano, R.J. Malloy, CFD Analysis on Aerodynamic Design Optimization of Wind Turbine Rotor Blades, World Academy of Science, Engineering and Technology/ 60/ 2009.
9. Travis Justin Carrigan, Aerodynamic shape optimization of a Vertical axis wind turbine, The University of Texas at Arlington,,December 2010.
10. A.V.Pradeep, Kona Ram Prasad, T.VictorBabu, Design And Analysis Of Wind Turbine Blade Design System (Aerodynamic).
11. S. RAJAKUMAR. et.al, computational fluid dynamics Of windturbine blade at various Angles of attack and low Reynolds Number.
12. Prof. John P. Sullivan, Ted Light & Jeffrey Robinson, AAE 415 – Aerodynamic Design Aerodynamic Design of a Large Horizontal-Axis Wind Turbine.
13. O`zlem ceyhan,Prof. Dr.canan o`zgen,Prof. Dr. `ismail h. Tuncer,Prof. Dr. `ismail h. Aerodynamic design and optimization of horizontal axis wind Turbines by using bem theory and genetic algoritm.
14. Franck Bertagnolio, NielsS_ensen, Jeppe Johansen and Peter Fuglsang , Wind Turbine Airfoil Catalogue,